Seasonal and Interannual Variability of the Oxygen Minimum Zone in the Gulf of California Entrance: Insights from High-Resolution Coupled Physical-Biogeochemical Modelling

Carlos Alberto Herrera-Becerril[1,2], François Colas[2,3], Joan-Albert Sanchez-Cabeza[4,*], José Martín Hernández-Ayón[5], Vincent Echevin[2], José Gilberto Cardoso-Mohedano[6], Ana Carolina Ruiz-Fernández[4]

1 Posgrado en Ciencias del Mar y Limnología, Universidad Nacional Autónoma de México; Av. Universidad 3000, Ciudad Universitaria Coyoacán, C.P. 04510, Ciudad de México, México. carlos.herrera.becerril@gmail.com
2 Laboratoire d'Océanographie et de Climatologie : Expérimentation et Approches numériques (LOCEAN), SU/IRD/CNRS/MNHN, Paris, France. vincent.echevin@locean.ipsl.fr
3 Laboratoire d'Océanographie Physique et Spatiale (LOPS), IRD/UBO/CNRS/Ifremer, IUEM, Plouzané, France. francois.colas@ird.fr
4 Unidad Académica Mazatlán, Instituto de Ciencias del Mar y Limnología, Universidad Nacional Autónoma de México, 82040 Mazatlán, Sinaloa, México. jasanchez@cmarl.unam.mx, caro@ola.icmyl.unam.mx
5 Instituto de Investigaciones Oceanológicas, Universidad Autónoma de Baja California, Carretera Ensenada-Tijuana 3917, Ensenada 22860, México. jmartin@uabc.edu.mx
6 Estación el Carmen, Instituto de Ciencias del Mar y Limnología, Universidad Nacional Autónoma de México, Carretera Carmen-Puerto Real km. 9.5, 24157 Ciudad del Carmen, Campeche, México. gcardoso@cmarl.unam.mx

* Corresponding author: jasanchez@cmarl.unam.mx

Abstract

The oxygen minimum zone (OMZ) in the Gulf of California entrance (GCE) is a crucial feature of the northeastern tropical Pacific, significantly influencing regional biogeochemical cycles and marine ecosystems. This study investigates the seasonal and interannual variability of the OMZ upper boundaries using a high-resolution physical-biogeochemical coupled model. The model results are evaluated against satellite observations, Argo profiles, and *in situ* data, demonstrating its capability to capture key dynamical processes, including mesoscale eddies, poleward undercurrents, and coastal-trapped waves (CTWs). The model reveals two alternating periods of shoaling and deepening of the OMZ boundary, modulated by the seasonal evolution of mesoscale dynamics and CTW propagation. El Niño Southern Oscillation (ENSO) events exert an evident influence, with El Niño causing a significant deepening and contraction of the OMZ, while La Niña leading to shoaling and expansion. The study highlights the complex interplay between local and remote oceanographic processes in determining the OMZ variability in the GCE. This research provides insights into the mechanisms driving OMZ dynamics in the Gulf of California and underscores the need for integrated observational and modeling approaches to predict the response of OMZs to ongoing climate variability.

Keywords: CROCO-PISCES model, dissolved oxygen, El Niño–La Niña variability, seasonal and monthly anomalies, marine environment

1. Introduction

Oxygen minimum zones (OMZs) are ocean areas with persistently very low dissolved oxygen (DO) concentrations (DO < 45 μmol kg^{-1}; Karstensen et al., 2008). They are typically found in the subsurface layer (100–900 m, below the mixed layer) in regions with poor ventilation and high surface primary productivity, which supplies large amounts of organic matter that depletes oxygen in the water column as it is degraded, such as at the eastern boundaries of the tropical oceans (*e.g.*, the eastern tropical Pacific, the eastern tropical Atlantic, and the northern Indian Ocean) (Helly & Levin, 2004; Karstensen et al., 2008). Although it is estimated that OMZs occupy only 7% of the total ocean volume, they are highly relevant for the ocean biogeochemical cycles (Paulmier & Ruiz-Pino, 2009). These zones are estimated to contribute ~35% of net ocean nitrogen loss by denitrification and anammox processes (Devol et al., 2006; Ward et al., 2009) and are responsible for ~30-50% of the N_2O emission to the atmosphere, an important greenhouse gas (Bange, 2008; McCoy et al., 2023). OMZs significantly influence the ocean's ecosystems, acting as a biological barrier for most aerobic organisms, including most fishes and species of economic interest (Helly & Levin, 2004; Diaz & Rosenberg, 2008; Gallo & Levin, 2016).

The OMZ of the northeastern tropical Pacific (NETP) is one of the most intense and extensive in the ocean (Karstensen et al., 2008; Stramma et al., 2008). Its spatial extension depends on the oxygen threshold chosen to define the OMZ. Considering the 45 μmol kg^{-1} threshold, the OMZ in this area extends along the eastern tropical Pacific from the coast of Baja California Peninsula (~25 °N) in the north down to the Ecuador coast in the south (0 °), where it mixes with the OMZ of the eastern tropical south Pacific (ETSP) (Paulmier & Ruiz-Pino, 2009). Off the Mexican Pacific coast, particularly in the Gulf of California, the OMZ penetrates along the gulf up to the large islands zone (~28 °N) and is typically found in a depth ranging from ~100 to ~600 m (Delgadillo-Hinojosa et al., 2006; Trucco-Pignata et al., 2019). However, in certain areas close to the coast, it can be observed at depths as shallow as ~50 m, and even in the coastal area due to wind-induced upwelling events (Márquez-Artavia et al., 2019; Herrera-Becerril et al., 2022).

The OMZ boundaries are delimited by a complex interaction between biochemical processes, such as microbial respiration (Kalvelage et al., 2015; Bretagnon et al., 2018), and dynamical processes, such as ventilation and horizontal advection of oxygenated waters from adjacent waters (Fuenzalida et al., 2009; Brandt et al., 2015). Processes like coastal upwelling, mesoscale eddies, and coastal trapped waves (CTWs) influence the OMZ upper boundary by inducing vertical displacements of the oxygen-rich mixed layer and shoaling or deepening the oxycline (Vergara et al., 2016; Auger et al., 2021; Espinoza-Morriberón et al., 2019). Climate phenomena, such as El Niño Southern Oscillation (ENSO), also influence the interannual variability of the OMZ boundaries, mostly modifying the largescale and mesoscale circulation patterns and therefore, the biochemical processes (Espinoza-Morriberón et al., 2019; Trucco-Pignata et al., 2019).

This study aims to analyze the seasonal and interannual variability of the Oxygen Minimum Zone (OMZ) boundary at the Gulf of California entrance (GCE) and to untangle the dynamic processes driving this variability. To achieve this, we implemented a regional configuration of the coupled hydrodynamical-biogeochemical model CROCO-PISCES (Coastal and Regional Ocean COmmunity model - Pelagic Interactions Scheme for Carbon and Ecosystem Studies) in the northeastern tropical Pacific (NETP), conducting a 13-year simulation (2008–2020) and a sensitivity analysis to remote forcings. This is the first time a physical-biogeochemical coupled model, like CROCO-PISCES, is used to study the seasonal and interannual variability of the OMZ boundary in the Gulf of California.

2. Study Area

The Gulf of California entrance (GCE) is the zone delimited by the virtual lines between the tip of the Baja California Peninsula (Cabo San Lucas) to El Dorado, Sinaloa (~24 °N on the mainland side) (the mouth line) and from Cabo San Lucas to Cabo Corrientes (~20.5 °N) (Lavín & Marinone, 2003). This region is a complex transition zone where different currents and water masses converge. In the surface layer, ramifications of the cold and low-salinity California Current Water (CCW; Table 1) reach the area mainly in winter and spring, interacting with the warm and high-salinity Gulf of California Water (GCW) and the warm and low-salinity Tropical Surface Water (TSW). In the subsurface, the nutrient-rich, oxygen-depleted, and saltier Subtropical Subsurface Water (StSsW) overlays, enriched with nutrients, and the colder, oxygen-depleted Pacific Intermediate Water (PIW) (Lavín & Marinone, 2003; Portela et al., 2016; Trucco-Pignata et al., 2019).

This area is characterized by several dynamic processes that could influence the OMZ boundary. On the continental side of the GC, the occurrence of wind-driven coastal upwelling, mainly from fall to spring, shoals the thermocline/pycnocline and could raise the upper boundary of the OMZ, primarily near the coast (Herrera-Cervantes et al., 2007). This area is also influenced by the generation and propagation of mesoscale eddies, particularly near the Cabo San Lucas (23 °N) and Cabo Corrientes (20 °N) capes (Fig. 1), which are hotspots for eddy formation due to the interaction between currents and coastal irregularities (Kurczyn et al., 2012). Along the coast, the poleward propagation of coastal trapped waves (CTW) modulates the depth of the pycnocline and could also induce vertical displacements of the oxycline (Gutiérrez et al., 2014). These CTW typically originate from the equatorial region; however, wind gaps from the gulfs of Tehuantepec, Papagayo (Costa Rica), and Panama could also generate them (Spillane et al., 1987; Flores-Vidal et al., 2014). From Cabo Corrientes, some of the CTW continue along the coast inside the GC, while others can pass the Baja California peninsula tip and continue their poleward propagation along the outer side of the peninsula (Gómez-Valdivia et al., 2017). In the subsurface, the Mexican Coastal Current (MCC) flows poleward along the coast between Gulf of Tehuantepec (14 °N) and Gulf of California (~24 °N), mainly during spring and fall, when it is enhanced by the semiannual CTWs associated poleward current (Gómez-Valdivia et al., 2015). This poleward flux could advect oxygen-depleted StSsW water toward the GCE.

The interannual variability in the southern Gulf of California (SGC) is strongly influenced by ENSO, especially during winter, due to its connection to the Equatorial Pacific by the CTW corridor along the continental border and atmospheric teleconnections (Lavín & Marinone, 2003; Herrera-Cervantes et al., 2007; Sánchez-Cabeza et al., 2022). During La Niña phases, the main seasonal patterns are enhanced: upwelling-favorable winds are intensified, and the thermocline is shoaled, resulting in cooler, nutrient-rich waters near the coast. In contrast, during El Niño phases, the relaxation of upwelling-favorable winds deepens the thermocline, bringing warmer, nutrient-poor waters to the surface and reducing biological productivity (Herrera-Cervantes, 2007; Lluch-Cota et al., 2010; Páez-Osuna et al., 2016).

Table 1. *Water masses in the Gulf of California; CCW: California Current Water, TSW: Tropical Surface Water, GCW: Gulf of California Water, StSsW: Subtropical Subsurface Water, PIW: Pacific Intermediate Water, PDW: Pacific Deep Water. DO classification: oxygen-rich (>90 µmol kg^{-1}), oxygen-poor (45–90 µmol kg^{-1}), oxygen-depleted (<45 µmol kg^{-1}). Modified from Portela et al. (2016), updated with data from Trucco-Pignata et al. (2019).*

Water mass	Θ (°C)	Salinity (g kg^{-1})	Depth (m)	DO level
CCW	10-21	<34.6	0-150	Oxygen-rich
TSW	>25.1	<34.6	0-50	Oxygen-rich
GCW	>12	>35.1	0-150	Oxygen-poor - Oxygen-rich
StSsW	9-18	34.6-35.1	45-520	Oxygen-depleted
PIW	4-9	34.6-34.9	400-1000	Oxygen-depleted
PDW	<4	>34.5	>1000	Oxygen-poor

3. Methods

3.1. The physical-biogeochemical coupled model CROCO-PISCES

The Coastal and Regional Ocean Community model (CROCO; Hilt et al., 2020) was used to study the hydrodynamics in the NETP. CROCO solves the Primitive Equations based on the Boussinesq and hydrostatic approximations (Shchepetkin & McWilliams, 2005; Penven et al., 2006). It uses stretched terrain-following sigma vertical coordinates and an Arakawa-C horizontal grid. Horizontal advection of temperature and salinity is calculated using a third-order scheme (RSUP3) (Lemarié et al., 2012). Vertical mixing is parameterized using KPP parameterization (Large et al., 1994). For a detailed model description, the reader is referred to Shchepetkin and McWilliams (2005 and 2009).

The hydrodynamical model CROCO was coupled with the PISCES biogeochemical model (Pelagic Interaction Scheme for Carbon and Ecosystem Studies). PISCES simulates marine the biogeochemical cycles of carbon, nutrients (NO_3, PO_4, Si, and Fe), and dissolved oxygen (DO). PISCES has four living compartments split into two size classes (nanophytoplankton and diatoms, and microzooplankton and mesozooplankton, respectively) and three non-living compartments (semi-labile dissolved organic matter, small sinking particles, and large sinking particles) (Aumont & Bopp, 2006; Aumont et al., 2015). We used the default model parameters as detailed by Aumont et al. (2015).

CROCO-PISCES computes the oxygen evolution considering dynamical transport, biogeochemical processes (sources and sinks), and air-sea exchange. Dynamical transport considers horizontal and vertical advection, as well as vertical mixing. The biogeochemical processes include oxygen production by photosynthesis, consumption by dissolved organic matter remineralization, microzooplankton and mesozooplankton respiration, and nitrification (Aumont et al., 2015; see also Resplandy et al., 2012 and Espinoza-Morriberon et al., 2019). In this work, we only focus on oxygen variability driven by the physical processes (particularly advection) rather than the biogeochemical processes and air-sea exchange.

3.2. Model configuration

We used a rotated rectangular grid to minimize land points and align the right boundary with the continental margin. The model domain (named CAM9) extends from 13 °N, 134 °W in the northern left corner to 18 °S, 84 °W in the southern left corner, and 36 °N, 121 °W in the northern right corner, in front of California, to 10 °S, 78 °W in the southern right corner, in front of Peru (Fig. 1). Since the equatorially-forced CTWs highly influences the ETPM (Spillane et al., 1987), the domain's southern limit was chosen to include the continental border of the Pacific at the equator. The horizontal grid resolution was ~9 km, and the vertical discretization had 45 sigma layers, with finer resolution towards the surface. The bottom topography was interpolated from ETOPO2 (Smith y Sandwell, 1997) and smoothed to avoid potential errors in the pressure gradient (Shchepetkin and McWilliams, 2005).

3.3. Atmospheric forcings

We used the COARE3.0 bulk formulation (Fairall et al., 2003) to compute the wind stress and heat fluxes imposed at the air-sea interface of the dynamical model. The 10 m wind speed components, surface air temperature, specific humidity, precipitation rate, and shortwave and longwave downward radiation were obtained from ERA5 hourly products at 0.25 ° resolution (Hersbach et al., 2018), then averaged to daily means and interpolated onto the model grid. The Fe atmospheric deposition required for the PISCES model's surface forcing was calculated from Tegen and Fung's model results (1995), assuming constant values for iron content and solubility.

3.4. Open boundary conditions

The open ocean boundary conditions for the dynamical model (temperature, salinity, sea surface height, and velocity components) were obtained from the Mercator Ocean reanalysis (1/12°, daily products) (GLOBAL_MULTIYEAR_PHY_001_030), then averaged every five days and interpolated into the model boundaries grid (CMEMS, 2023).

The initial and open boundary conditions for the biogeochemical model (DO, NO_3, PO_4, SiO_3, DIC, total alkalinity, DOC, and dissolved iron) were obtained from the climatology of a NEMO-PISCES global simulation (Aumont et al., 2015). The surface forcings and the initial and boundary conditions were preprocessed using the CROCOTOOLS package (Penven et al., 2019).

3.5. Simulation running

We performed a 13-year control simulation (2008-2020). The spin-up was accomplished by repeating the year 2008 three times to reach a steady state, then the output was used as the initial condition (1 January 2008) for the control simulation. Model variables (outputs) were stored as five-day averages. To include an equal number of El Niño and La Niña events, the first two years (2008-2009) were discarded, and the analyses were performed from 2010-2020. This period includes El Niño periods 2014-2016 and 2018-2019, and La Niña periods 2010-2012 and 2016-2018.

To analyze the influence of remote oceanic forcings, particularly the equatorially-forced CTWs, on mesoscale dynamics and the OMZ boundary variability, we performed a sensitivity experiment. This involved running a simulation (named LFBRY) in which the ocean boundary forcings are yearly averages. The objective was to filter out seasonal and intra-seasonal variability while preserving the low-frequency interannual signal.

3.6. Model's performance evaluation

To evaluate the model's performance, the model results were compared with observations from different data sources (Table 2). The mean state was evaluated by comparing the modeled

annual and seasonal means of the sea surface temperature (SST) over the 2010 - 2020 period with the observed SST means from Operational Sea Surface Temperature and Ice Analysis (OSTIA) (Good et al., 2020). To evaluate the interannual performance, we compared modeled and observed (OSTIA) SST monthly anomaly time series averaged in the southern GC (Fig. S1). We also compared modeled and observed sea level anomaly (SLA) time series averaged in the same area (Fig. S2). We estimated the model skill (using the Willmott method; Willmott, 1981) and the root mean square error normalized to the range of model values (NRMSE) for both, monthly anomaly SST and SLA, time series comparison.

To evaluate the mesoscale activity, we calculated the standard deviation of the 95-day high-passed sea level anomaly (henceforth referred to as SLA-SD) during the 2010 - 2019 period. We compared it to the SLA-SD obtained from the AVISO (Archiving, Validation and Interpretation of Satellite Oceanographic data) satellite altimetry data, following the methodology from Liang et al. (2012).

To evaluate the modeled vertical structure, we compared the temperature and DO profiles from biogeochemical-ARGO floats (Claustre et al., 2020) with profiles from the nearest model grid at the same time. This analysis included 632 profiles from biogeochemical-ARGO floats. Since no biogeochemical ARGO floats were available in the GC during the simulation time period, we also compared the model temperature and DO with a transect along the GC sampled in June 2015 (Trucco-Pignata et al., 2019).

Table 2. Summary of data used in this work.

Name	Variables	Use	Reference
ETOPO2	Bottom topography	Model configuration	Smith & Sandwell, 1997
ERA5	10 m wind speed, air surface temperature, specific humidity, precipitation rate, and shortwave, longwave downward radiation	Model atmospheric forcings	Hersbach et al., 2018
Fe deposition	Fe atmospheric deposition	Model atmospheric forcings	Tegen & Fung, 1995
Mercator Ocean reanalysis (GLOBAL MULTIYEAR PHY 001 030)	Temperature, salinity, sea surface height, and velocity components	Initial and open ocean boundary conditions for the dynamical model	CMEMS, 2023
NEMO-PISCES global simulation	DO, NO_3, PO_4, SiO_3, DIC, total alkalinity, DOC, and dissolved iron	Initial and open boundary conditions for the biogeochemical model	Aumont et al., 2015

OSTIA	Sea surface temperature (SST)	Model validation	Good et al., 2020
AVISO+	Sea level anomaly (SLA)	Model validation	Pujol et al., 2016
ARGO biogeochemical floats	DO and temperature profiles	Model validation	Claustre et al., 2020
CRUISE data	DO and temperature	Model validation	Trucco-Pignata et al., 2019

4. Results

4.1. Model evaluation

The SST annual mean comparison with OSTIA showed a semi-uniform cold bias between -0.2 and -0.5°C in almost the whole domain, except in the areas close to the northern and southern boundaries, next to continental borders, where the bias was up to 1.2 °C (Fig. S1A). The comparison for JFM (January-February-March) SST showed a similar cold bias between -0.5 and -1 °C in the study area, except for the GC. There, the bias was positive, between 0-1 °C in the southern GC and 0.7-2 °C in the northern GC, close to the large islands (Fig. S1B). The JAS (July-August-September) comparison showed a moderate warm bias around the GCE (~0.5 °C) and a cool bias (-0.1 to -0.3°C) in the southern GC (Fig. S1C).

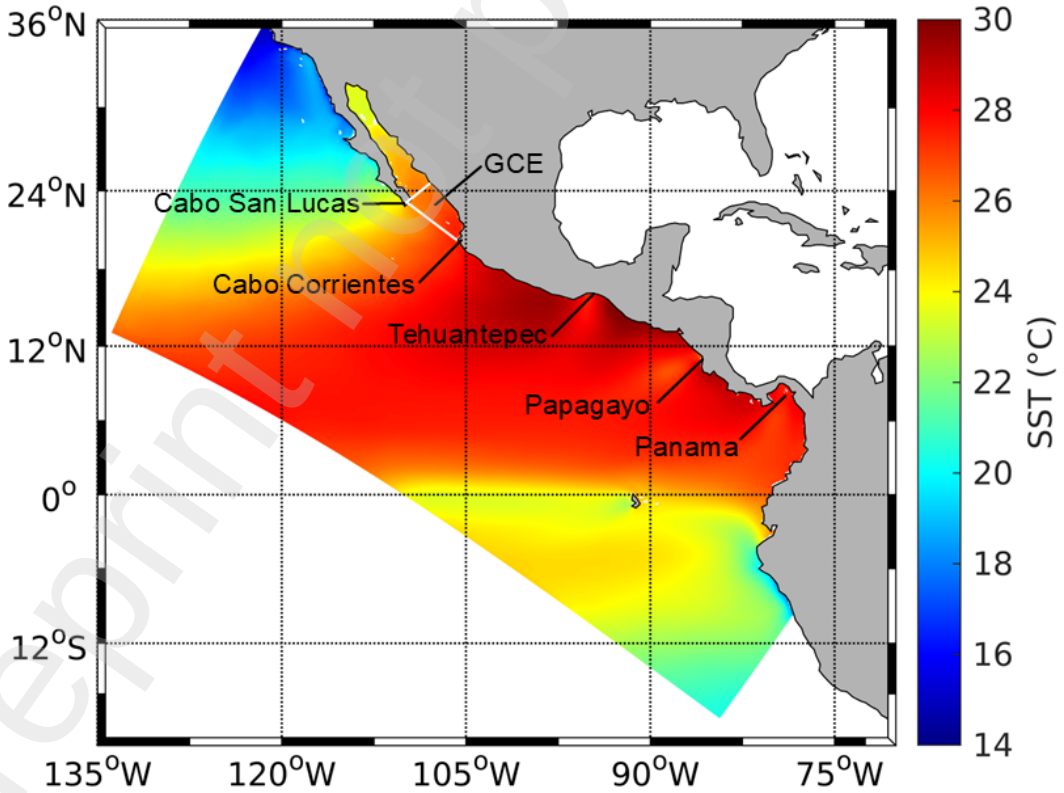

Fig. 1. *Domain of the CAM9 model, with mean CROCO SST calculated over the 2010 - 2020 period. White lines denote the Gulf of California entrance (GCE).*

The model well represented the ranges of intra-seasonal and interannual variations (Fig. S2). The model skill for the SST monthly anomaly in the selected area was 0.97 and the NRMSE was 0.06, which indicates good model performance. The strong cold anomalies in 2010 and 2011, as well as the warm anomalies in 2014 and 2015 associated with El Nino events, were well reproduced.

The SLA-SD comparison (Fig. 2) showed that the model's mesoscale variability is slightly lower than that derived from AVISO. However, the model simulates well the areas with significant mesoscale activity, such as the tip of the Baja California Peninsula and Cabo Corrientes (Fig. 1) (Kurczyn et al., 2012). The SLA time series comparison between the model and AVISO in the south GC showed a model skill was 0.96 and an NRMSE of 0.08 (Fig. S3).

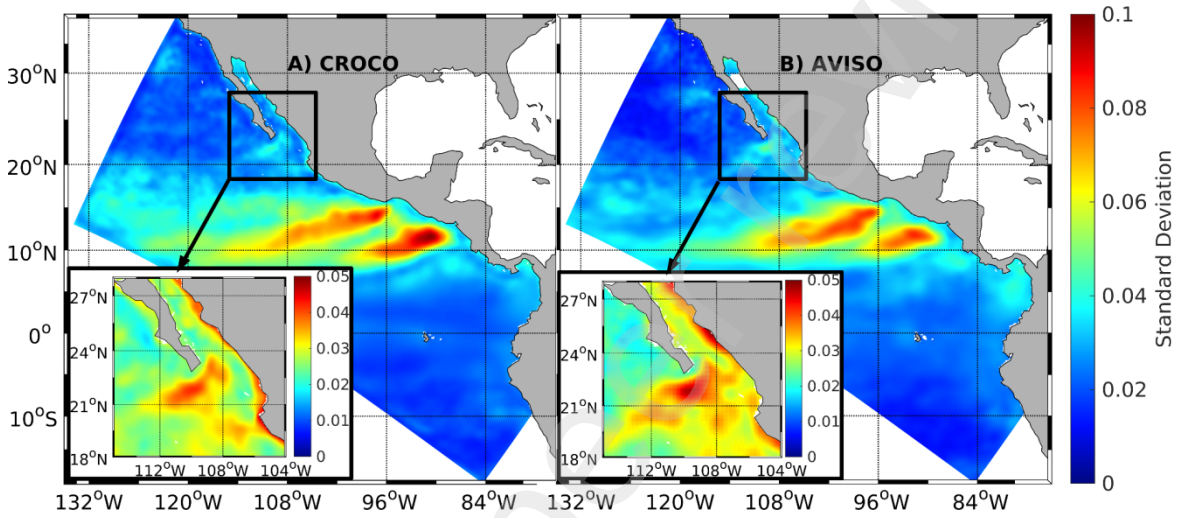

Fig. 2. *Standard deviation from 95-day high-passed sea level anomaly (SLA-SD) from A) CROCO and B) AVISO altimetry data (2010-2019).*

The comparison with ARGO profiles showed that the model was able to estimate the thermocline depth correctly albeit slightly more diffusive (Fig. 3B). The modelled and observed oxyclines were of similar intensity (~4 µmol kg^{-1}/m) but deeper in the model (Fig. 3). The mean difference of the oxycline depth (depth difference for each DO from 20 to 200 µmol L^{-1}) between selected CROCO and ARGO profiles was 17.1 ± 0.1 m. The NRMSE for the CROCO profiles compared to ARGO from surface to 250 m depth was 0.17 for DO and 0.08 for temperature.

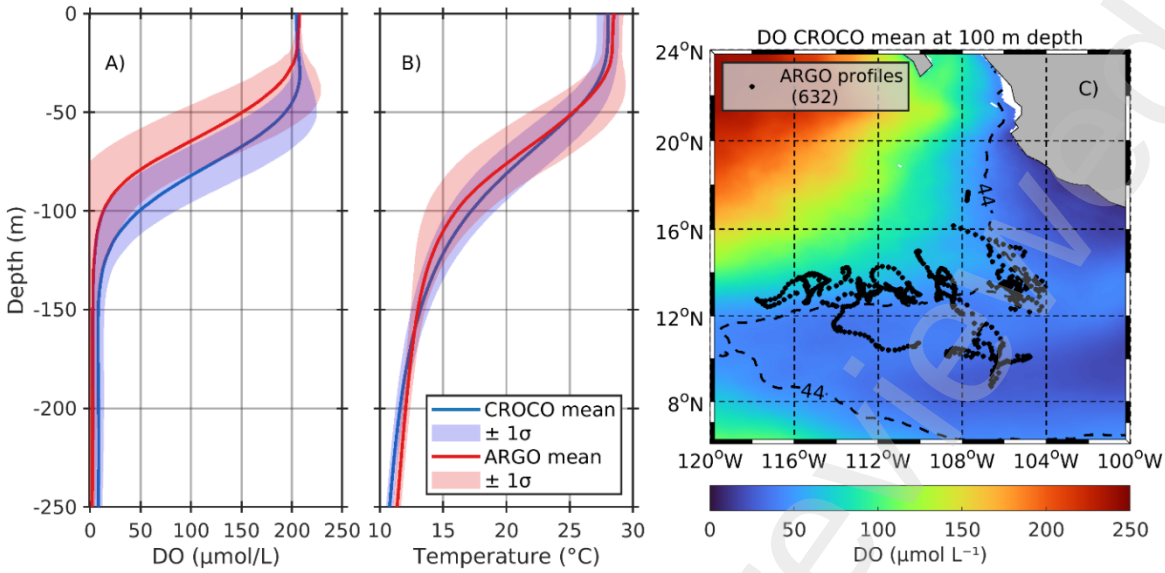

Fig. 3. *Comparison of the CROCO model results with ARGO floats. A) Dissolved oxygen (DO) and B) temperature means from all available profiles. C) Map with the location of ARGO profiles and DO from the model at 100 m depth. The dashed line remarks the limits of oxygen minimum zone (OMZ) (44 µmol L^{-1}) at that depth.*

The comparison of DO and temperature transect along the GC, confirmed that the modeled oxycline was deeper and more diffuse than the observed, but nevertheless reproduced some of the observed latitudinal patterns of temperature and the upper limit of the OMZ (44 µmol L^{-1}), particularly the front around 24 °N (Figs. S4 & S5).

In the following, we explore the variability of the OMZ in the GCE and discuss the processes responsible for it based on the model results. The impact of the afore-mentioned DO bias is discussed in the last section.

4.2. Seasonal variability

Several DO thresholds have been used to define the OMZ boundaries according to different criteria. Here, we use the 44 µmol L^{-1} DO concentration to define the upper limit of the OMZ, referred to hereafter as OMZ-top. This threshold is reported to be a limit below which most of the epipelagic species suffer stress, so it can be considered an ecosystem boundary (Hoffman et al., 2011). A similar threshold (44 µmol kg^{-1}) has been used in previous studies in the same zone (Sánchez-Velasco et al., 2017; Trucco-Pignata et al., 2019; Sánchez-Pérez et al., 2021). We also used the 22 µmol L^{-1} isopleth, also reported as the "severe hypoxia" threshold, to identify the OMZ core in the model results, hereafter referred as OMZ-core (Helly & Levin, 2004; Diaz & Rosenberg, 2008; Hoffman et al., 2011).

In the Mexican Pacific coast, the OMZ-top is shallower (<100 m) next to the coast up to Cabo Corrientes (Fig. 4), then it deepens to the north along the GC up to ~250 m depth around 28 °N, at the south of the large islands. The major seasonal variation of the OMZ-top occurs next to the continental border on the mainland side of the GC (Fig. 4). To visualize the OMZ boundary variability (OMZ-top and OMZ-core) along the continental border, we defined a transect along the 500 m isobath next to the mainland coast (Fig. 4C) and plotted the DO mean concentration over the 2010 - 2020 period (Fig. 5) and the monthly means (Fig. S6).

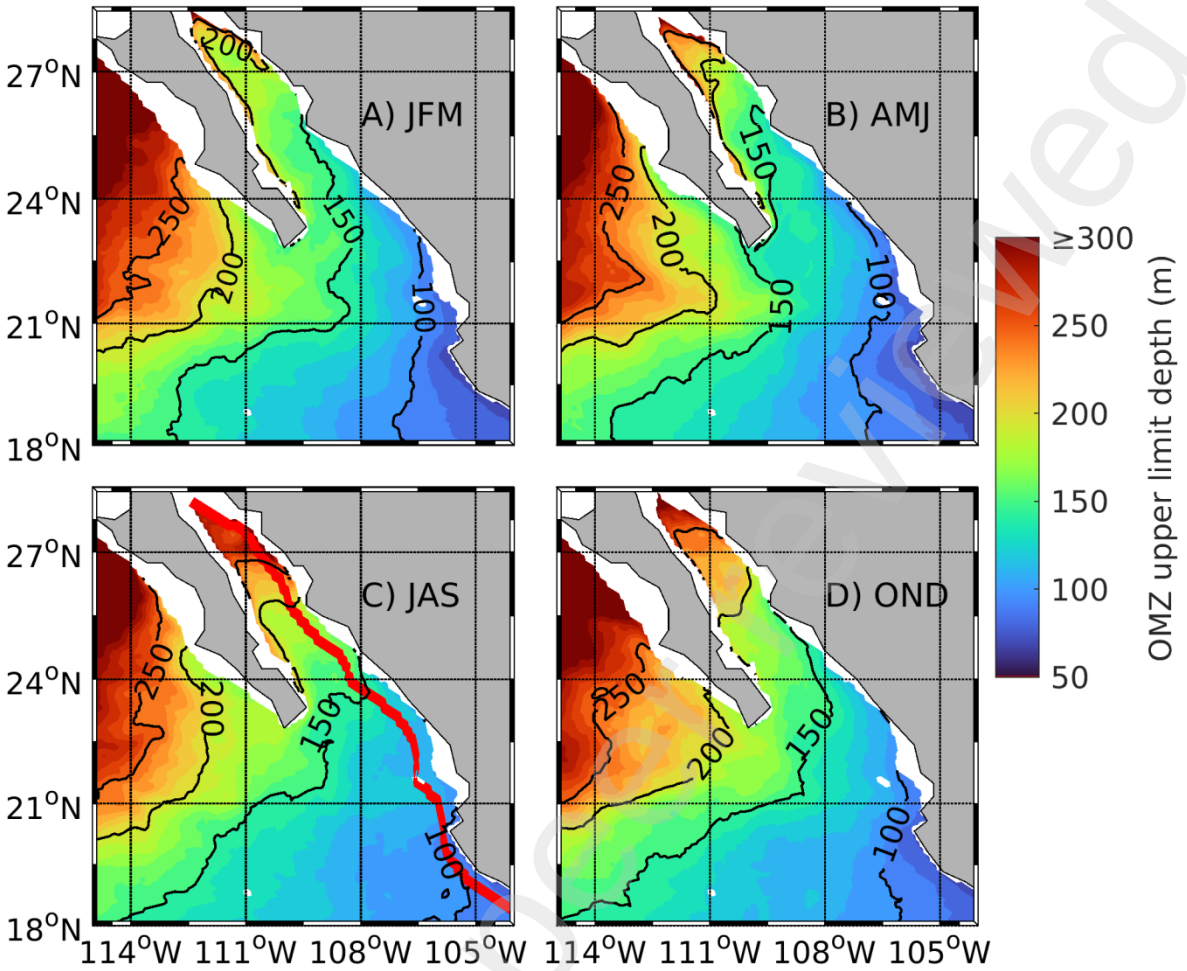

Fig. 4. *Seasonal means of the depth of the OMZ upper limit (DO = 44 µmol L^{-1}) during the 2010-2020 period: A) January-February-March, B) April-May-June, C) July-August-September, and D) October-November-December. The red line along the Gulf of California in C) shows the position 500 m isobath selected to draw the vertical section in Fig. 5.*

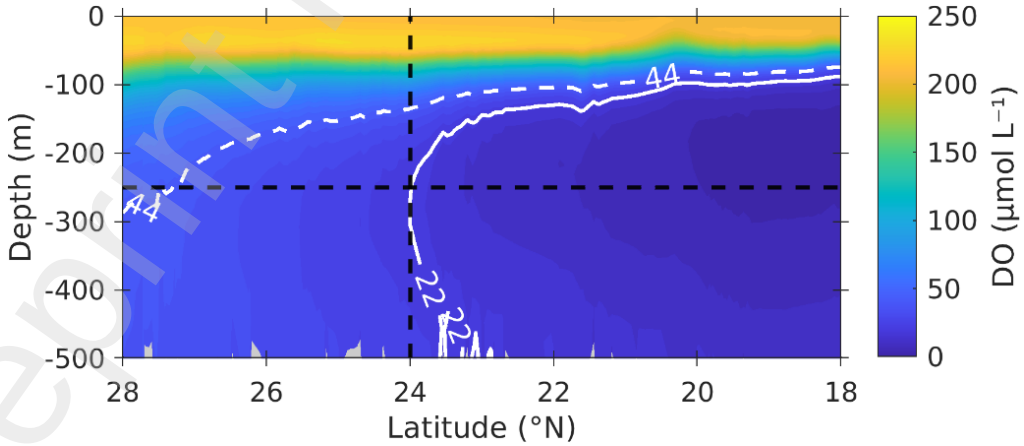

Fig. 5. *Mean of dissolved oxygen (DO) concentration, over the 2010 - 2020 period, along a vertical section following the 500 m isobath in the continental side of the Gulf of California, (Fig. 4C). Dashed line marks the 44 µmol L^{-1} isopleth (OMZ-top), and continuous line marks the 22 µmol L^{-1} isopleth (OMZ-core). The horizontal dashed line marks the 250 m depth,*

and the vertical line at 24 °N denotes where this transect crosses the Gulf of California mouth.

The monthly means of the OMZ-top and OMZ-core along the 500 m isobath transect revealed a semiannual pattern of two alternating periods of shoaling and deepening of the OMZ-top and poleward expansion and contraction of the OMZ-core (Fig. S6). The first shoaling/expansion period occurs from October to January and reaches its maximum in December. During this period, the OMZ-top shoals along the coast, between ~20.5 °N (Cabo Corrientes) and ~25 °N (Topolobampo) (Fig. 4D), and the OMZ-core extends northward, reaching its seasonal maximum position (~24.75 °N). Later in winter (February and March), the model shows a weak deepening of the OMZ-top and contraction of the OMZ-core to the south, just around the GC mouth. During spring (April-May), the model shows a second and strongest period of shoaling and poleward expansion of the OMZ boundary, with a maximum in May. In this period, the OMZ-top is shallowest, and the OMZ-core reaches its northernmost position (~25 °N).

In summer (JAS), the model shows a second and the most intense period of southward contraction, when the OMZ-top is progressively deepened to the north of ~27 °N, where it abruptly sinks from ~200 m to ~400 m, creating a front-like pattern. Unlike during other seasons, the summer deepening of the OMZ-top occurs rather homogeneously across the gulf width around the GC mouth (Fig. 4C). In summer, the OMZ-core rapidly contracts to the south; from July, the OMZ-core is positioned outside of the GC and reaches its southernmost position in September (~23 °N; Fig. S6). Figure 6 summarizes this seasonal cycle by showing the monthly means of the OMZ-top at the GC mouth latitude (24 °N) in the alongshore transect (Fig. 5) and the OMZ-core northernmost position reached along the same transect. Intraseasonal CTW had a weak impact on the variability of the OMZ boundary position, as the LFBRY simulation showed similar results to the control simulation albeit smoother transitions in the range variation of OMZ-top depth and OMZ-core northern position, particularly during the summer contraction (Figs. 6A&B).

4.3. Interannual variability

To compare the influence of El Niño/La Niña events on the OMZ boundary, we calculated seasonal means of the OMZ-top and OMZ-core position during La Niña 2010-2011 and El Niño 2015-2016, both of which were strong events (Sanchez-Cabeza et al., 2022; Boening et al., 2012). During La Niña, the OMZ-top was ~50 m shallower than average in almost all the SGC (Figs. 7A,C & 8B), and the alongshore OMZ-core was slightly shallower than the climatology, reaching a position around one further north (Fig. 8B).

In contrast, during El Niño 2015-16, the OMZ deepened in the GC. During fall (OND-2015), the OMZ-top was deeper than the average (Figs. 7B,D & 8A). In winter (JFM-2016), the OMZ-top was deeper, and the OMZ-core showed a marked deviation from the seasonal mean, being positioned in a front-like pattern, out of the GC mouth, southern than 22 °N (Fig. 8B).

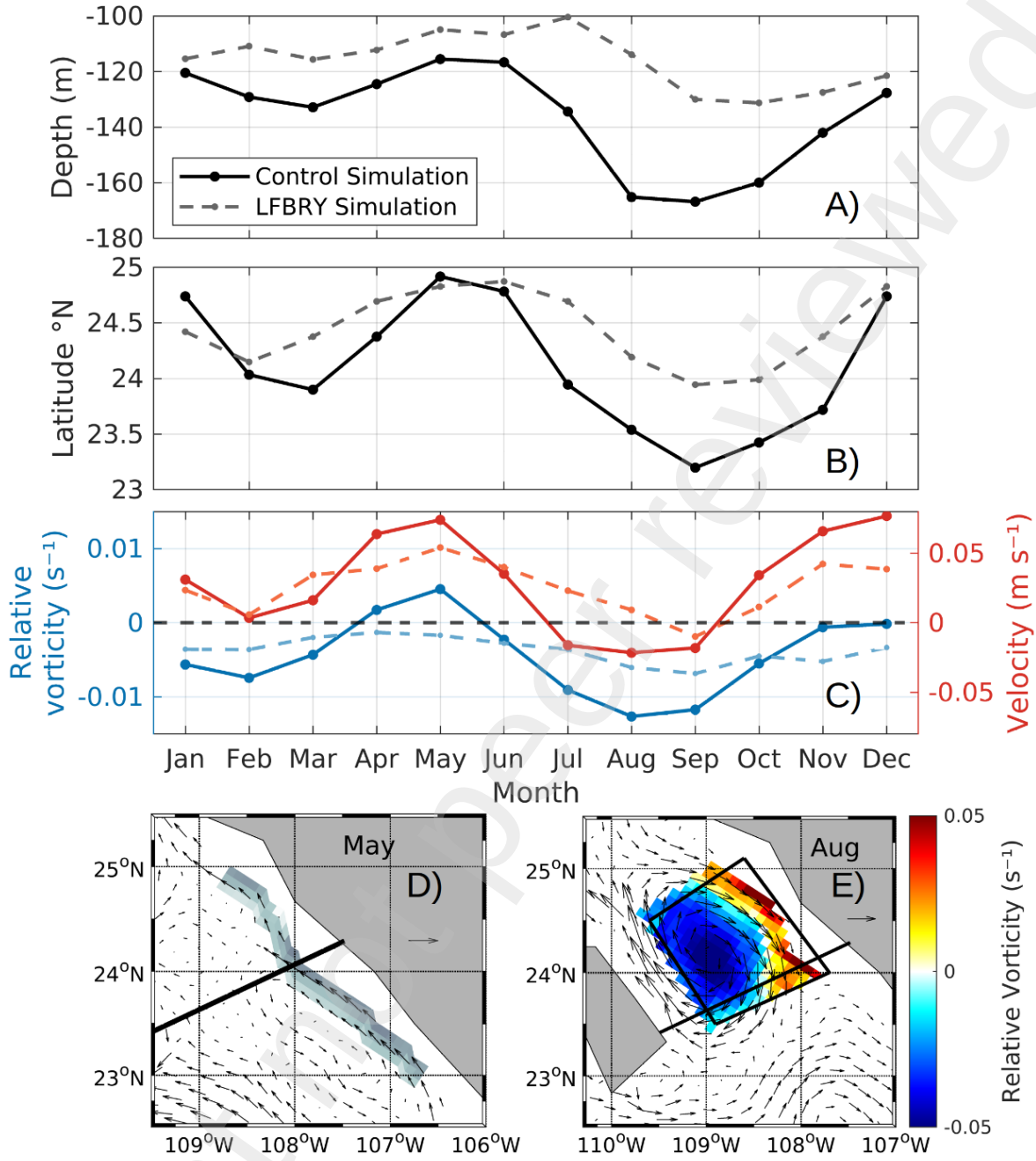

Fig. 6. *Seasonal cycle of A) mean depth of OMZ-top (44 µmol L^{-1}) at 24 °N in the transect along the coast in Fig. 5. B) Seasonal cycle of the northernmost position reached by the OMZ-core (22 µmol L^{-1}) at 250m in the same transect. C) Relative vorticity (blue) in the area inside the box in E), and mean velocity (red) in the transect along the coast in D).*

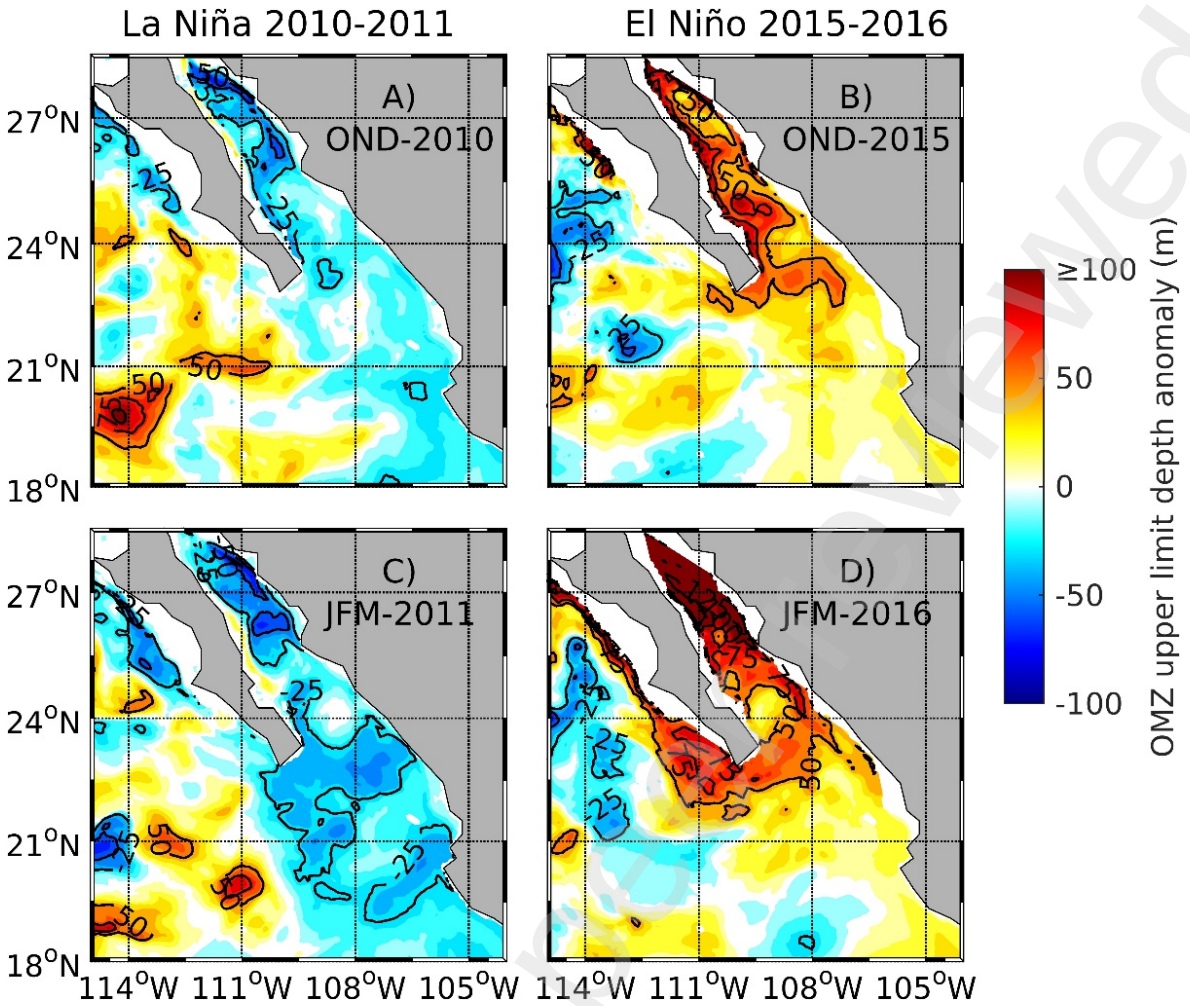

Fig. 7. Comparison of the OMZ upper limit (44 μmol L-1) between La Niña 2010-2011 (left column: a,b) and El Niño 2015-2016 (right column:c,d) during fall and winter.

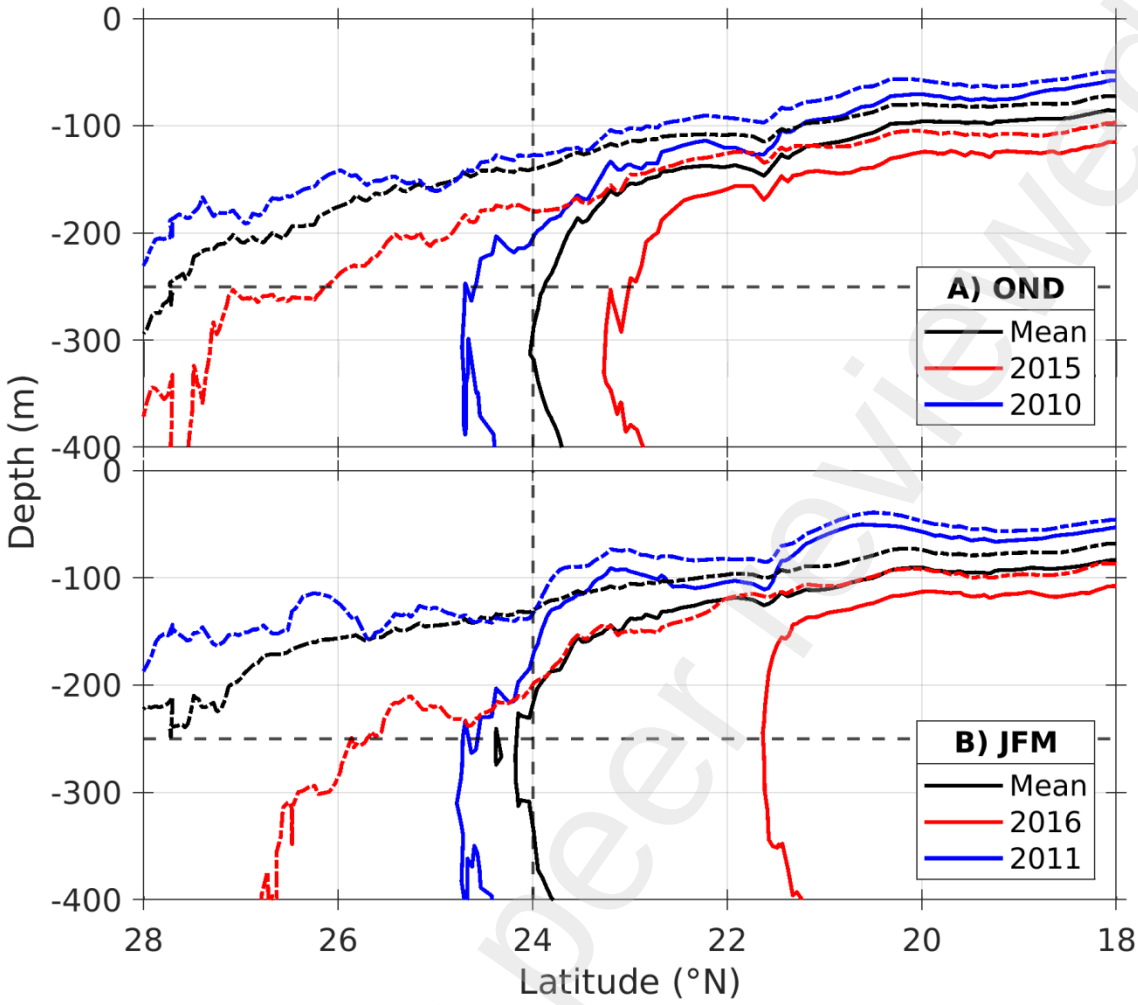

***Fig. 8**. Quarterly means of the position of the OMZ-top (44 µmol L^{-1}, dashed line) and OMZ-core (22 µmol L^{-1}, continuous line) along the 500 m isobath transect (shown in Fig. 4) in A) fall (OND) and B) winter (JFM), during El Niño 2015-16 (red line) and La Niña 2010-11 (blue line).*

CTWs are one of the mechanisms through which the ENSO signal is propagated from the Equatorial Pacific to the CG, and its passage can be observed as anomalies of sea level. The Hovmöller plot of the SLA and OMZ-top anomalies along the 200 m isobath next to the Mexican Pacific (Fig. 9D) coast shows two periods of positive (downwelling) and negative (upwelling) anomalies in both variables, which coincides with El Niño 2015-16 and La Niña 2010-11 events (Figs. 9A,B). The SLA anomalies showed a continuous pattern along all the transect, which suggests that the CTWs propagate along the Mexican Pacific coast. In contrast, the OMZ-top anomalies are more diffuse, particularly at the north of 22 °N (Fig. 9A). To analyze the influence of the CTW in the OMZ-top variability, we calculated the cross-spectrum of SLA and OMZ-top anomalies in different points south (19 °N) and north (23 °N) of Cabo Corrientes (see Fig. 9D). This cross-spectrum showed a peak of shared energy near ~55 days at 19 °N. Still, the peak did not exist at 23 °N. Expectedly, the peaks were not observed in the spectrums from the LFBRY simulation (Fig. 9E).

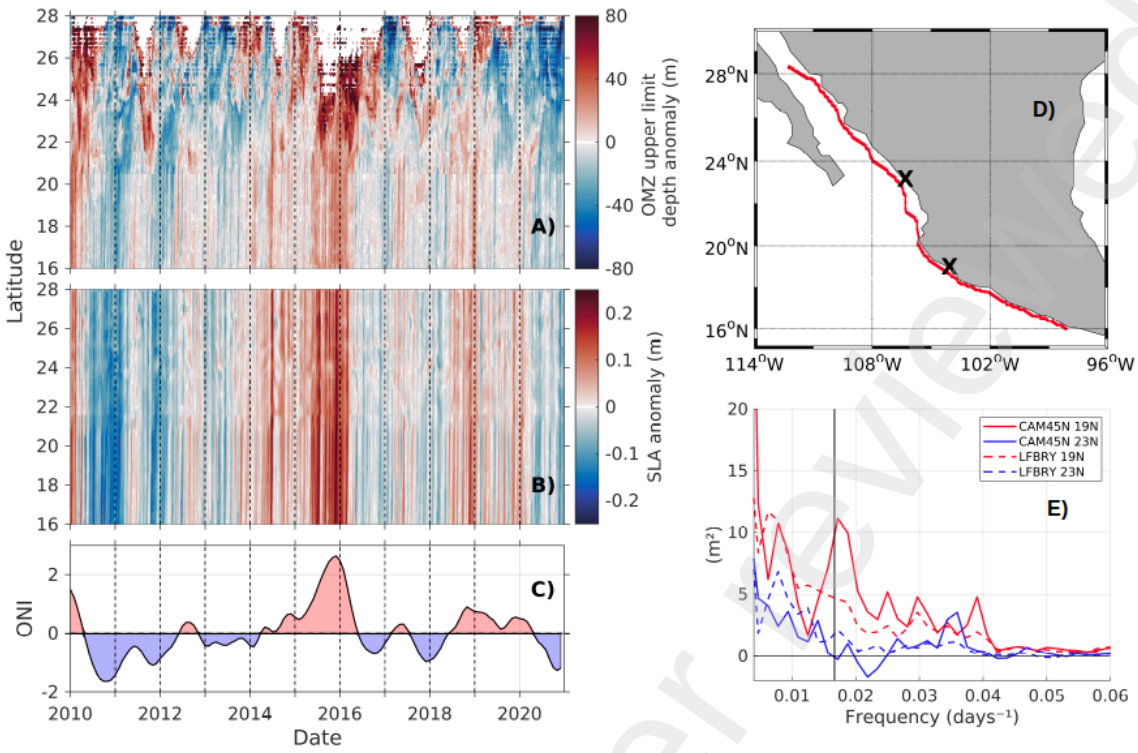

Fig. 9. *Hovmöller plots of the A) OMZ upper boundary anomaly and B) sea level anomaly (SLA) along a transect following the 200 m isobath along the Mexican Pacific coast, and C) the Oceanic Niño Index (ONI) time series. D) Transect along the 200 m isobath; X marks show the 19 and 23 °N locations, where the SLA and OMZ top anomalies time series were extracted to calculate the cross-spectra (E). The masked values in the upper panel (A) correspond to strong positive anomalies when OMZ-top is no longer defined (DO is larger than 44 μmol.kg^{-1} over the entire water column).*

5. Discussion

Our model simulation adequately captured the seasonal and intraseasonal variability of physical variables (SST and SSH), suggesting that the main dynamical processes are correctly simulated (Figs 2, S1, S2 & S3). However, as the model estimated a deeper oxycline than observations (Figs. 3, S4), the exact position of the OMZ-top and the OMZ-core is expected to be shallower than simulated. Our simulation also reproduced well the latitudinal variations of the OMZ boundary (Figs. S4 & S5) and can thus be useful in studying the dynamical processes driving these variations, as abundant observations are not abundant in the region. In fact, to date, not a single biogeochemical ARGO float with available oxygen measurements has been deployed in the GC, and the World Ocean Atlas climatology of DO includes very few observations in the region (Garcia et al., 2024).

5.1. Transition area and decoupling

The OMZ-top and the OMZ-core have similar temporal variability but different spatial behavior along the GCE and SGC. Cabo Corrientes acts as a tipping point where the transition area starts. To the south of the cape, the isopleths are close while to the North the isopleths decouple: the OMZ-top remains visible along all the SGC, up to the large islands, while the OMZ-core rapidly deepens, creating a front-like pattern at depths from ~150 to ~400 m, with a latitudinal variability around the GC mouth (from ~23 to 25 °N) (Fig. 5&S6). A similar

decoupling pattern has been observed by Cepeda-Morales et al. (2013) in a transect perpendicular to the coast at the Cabo Corrientes latitude. This decoupling could be a characteristic of a transitional area.

5.2. Influence of poleward undercurrent

The seasonal variability of the OMZ boundary along the continental side of the GCE is mainly related to subsurface circulation patterns, particularly with the alternated periods of semiannual poleward undercurrent occurring in fall and spring and the formation of an anticyclonic eddy in the GC mouth during winter and summer (Fig. 10) (Kessler, 2006; Zamudio et al., 2008; Godínez et al., 2010; Gómez-Valdivia et al., 2015). In the GCE, the poleward undercurrent, which is part of the Mexican Coastal Current flows in a narrow strip along the continental slope from October to January (fall) and from April to June (spring) (Fig. 10*)*. It has a maximum velocity of ~0.1 m s^{-1} at depths from ~100 m to ~400 m, approximately in the same depth range of the StSsW is found (Lavín et al., 2013) (Fig. 11). This flows advects low DO waters from the OMZ northward, pushing the OMZ-core inside the GC, and shoaling of the OMZ-top. The months of maximum poleward flow, December and May, coincide with the northernmost position reached by the OMZ-core, up to ~25 °N along the coast (see Fig. 6B).

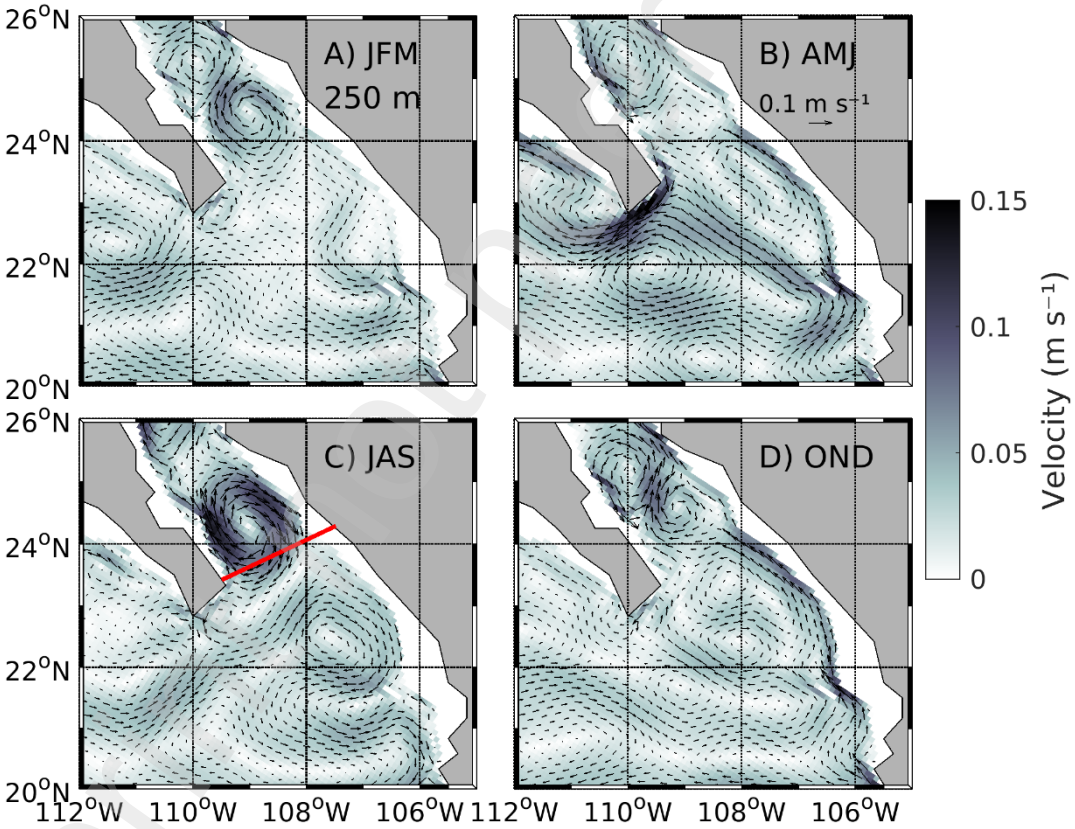

Fig. 10. *Seasonal means of circulation at 250 m depth during 2010 - 2020. The red line in C) shows the position of the transect across the GC mouth used in Figs. 11 & 12.*

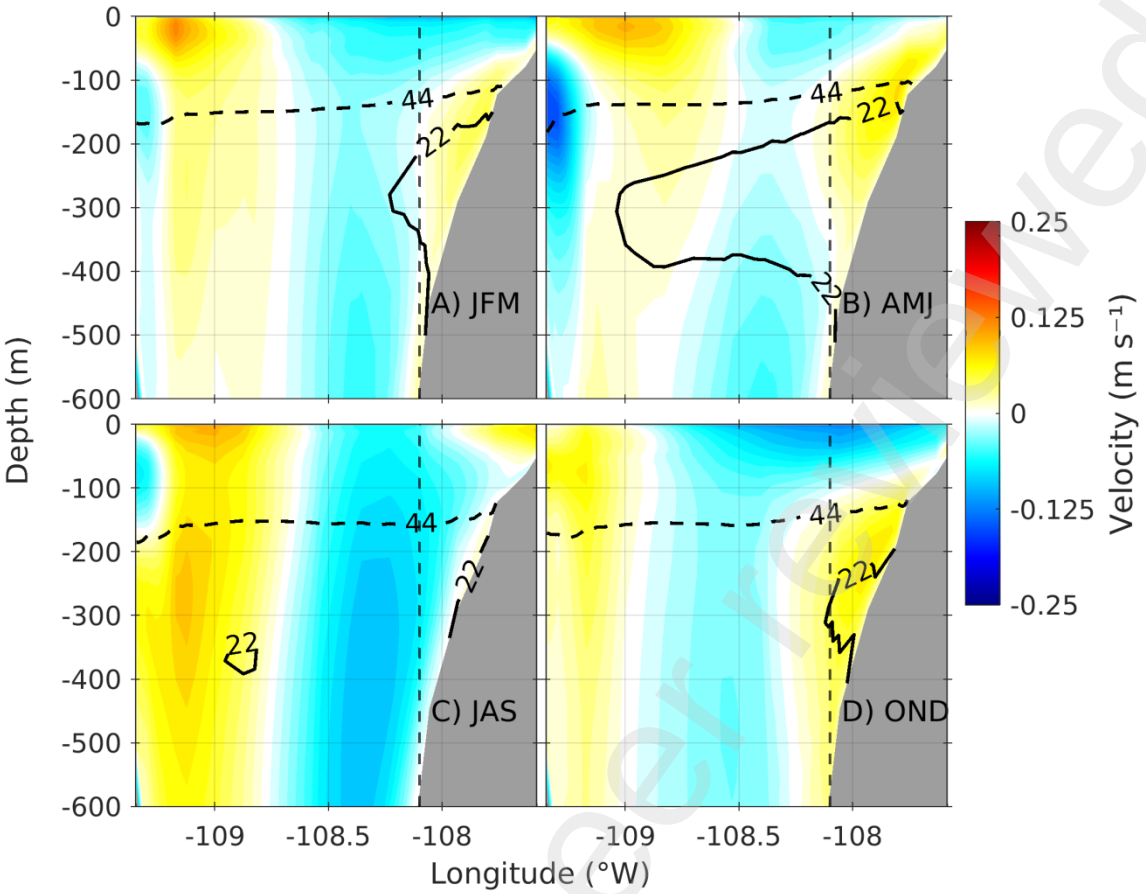

Fig. 11. *Seasonal means of velocity perpendicular to the transect across the GC mouth (Fig. 10C). The positive (negative) values indicate poleward (equatorward) flow, the dashed line shows the DO = 44 µmol L^{-1} isopleth, and the continuous line shows the DO = 22 µmol L^{-1} isopleth.*

5.3. Influence of an anticyclonic eddy at the GC mouth

Approximately one month after each poleward flow peaks, an anticyclonic eddy begins to form in the SGC, as part of an eddy train formed along the GC axis (Fig. 10). This eddy is particularly intense in summer (Fig. 10C). These eddies extend up to 700 m depth, and the difference in their properties (salinity, temperature, and DO) is more delimited in the subsurface (~300 m). Their maximum velocities (up to ~0.14 m s^{-1}) are found from 200 to 600 m during August-September (Pegau et al., 2002; Zamudio et al., 2008; Lavín et al., 2013). Our model results agree with these observations (Fig. 11C).

It has been proposed that the eddy train is formed by baroclinic instabilities caused by the interaction of the poleward undercurrent, intensified by the passage of CTWs, with topographic irregularities (Zamudio et al., 2008). Since the poleward flow is stronger in spring than in fall, this hypothesis is consistent with the more intense anticyclonic eddy formed in the GC in late summer than that formed in winter (Figs. 10A&C). It has also been suggested that some eddies in the south of GC could be formed by localized wind impulses and by instabilities caused by the interaction between currents (Lavín et al., 2009; Pantoja et al., 2012). The results of our sensitivity experiment with filtered remote forcing (LFBRY) showed that a much weaker summer eddy is also formed in the absence of intra-seasonal equatorially-forced CTW (Fig. S7). This supports the hypothesis that CTWs enhance the poleward flow and intensify the eddy train but are not crucial to its formation (Zamudio et al., 2008).

The position of the anticyclonic eddy, close to the GC mouth, provokes a subsurface inflow to the GC by the peninsula side and an outflow by the continental side (Fig. 10A&C), forcing the OMZ-core out of the GC mouth along the mainland side. Our results suggest that a weaker winter anticyclonic eddy is also formed at the GC mouth (Fig. 10A) and could be responsible for the weak deepening of the OMZ-top and the less-pronounced contraction of the OMZ-core in February and March (Fig. 6). Contrarily, the winter wind acts in the opposite way, shoaling the OMZ-top by the influence of wind stress curl and wind-induced coastal upwelling (Lavín & Marinone, 2003; Zamudio et al., 2008).

North of 26 °N the deepening of the OMZ-top during summer is more pronounced, creating a front-like pattern, very likely to be caused by interaction between the oxygenated Gulf of California Water (GCW) and the poor-oxygenated Subtropical subsurface water (StSsW) (Lavín & Marinone, 2003; Trucco-Pignata et al., 2019). While the poleward undercurrent next to the continental border is narrow, the outflow due to the anticyclonic eddy is wider and covers the eastern half of the GC mouth (Figs. 10 & 11). This explains why the isolines of the OMZ-top tend to be aligned with the gulf axis during the expansion periods while they tend to be perpendicular to the gulf's axis during the contraction in summer (Fig. 4).

5.4. Interannual variability

The characteristics of the OMZ boundary during strong El Niño and La Niña events showed marked deviations from the average conditions, mainly in winter (JFM). Most of the differences were related to changes in the subsurface dynamics that dominate the seasonal patterns, i.e., the semiannual poleward undercurrent and the anticyclonic circulation at the SGC.

During La Niña 2010-2011, the OMZ-top was slightly shallower than average, and the OMZ-core reached ~1° farther north inside the GC, both in fall and winter (Fig. 8). However, the poleward undercurrent, responsible for advecting the OMZ-core inside the GC, was not stronger than average, so the OMZ position difference was not caused by an enhanced poleward flow (Fig. 12A, B). During La Niña 2010-11, a sequence of upwelling CTWs reached the GC (Fig. 9B) which could cause the observed intensification in the anticyclonic eddy in the SGC (S8A,C). However, this eddy was shallow (~100 m depth) (Fig. 12D), so neither participated in the contraction of the OMZ-core. Furthermore, during the previous summer (2010), the subsurface circulation at the GCE, including the anticyclonic eddy in the mouth, was weaker than average (not shown). Therefore, the OMZ-core expulsion from the GC by this eddy was also weaker, so when the following expansion period in winter started, the OMZ-core was already closer to the GC mouth.

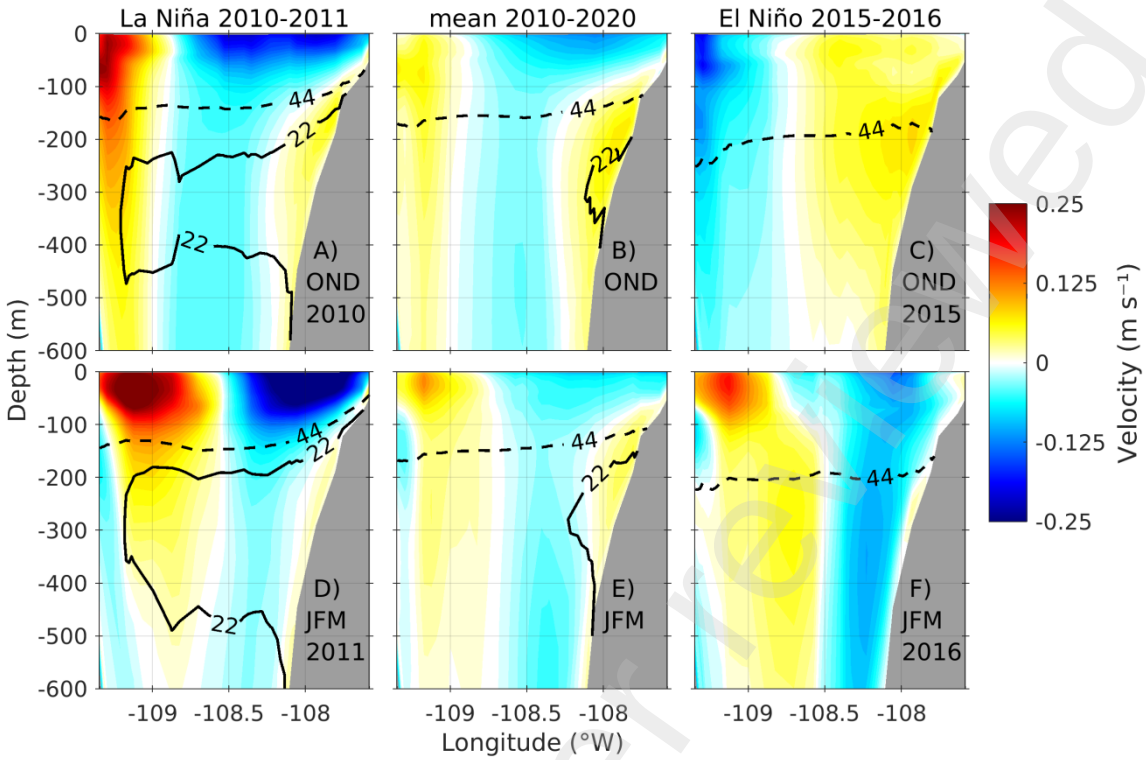

Fig. 12. *Comparison of the transect of the velocity perpendicular to the GC mouth during OND (upper panel) and JFM (lower panel) of La Niña 2010-2011 (left column), mean over the 2010 – 2020 period (middle column) and El Niño 2015-2016 events (right column).*

El Niño affects the GC by i) propagating downwelling CTWs, ii) decreasing upwelling favorable winds, and iii) enhancing the advection of tropical surface water (TSW) to the north (Herrera-Cervantes et al., 2007; Lluch-Cota et al., 2010). El Niño 2015-16 was one of the strongest events recorded and was preceded by an anomalous warm episode in 2014-2015 (Sanchez-Cabeza et al., 2022). The model showed a period of propagation of downwelling CTWs, which started in 2014, intensified during fall-winter 2015-16 and coincided with deepening periods of the OMZ-top. The observed peak of shared energy (period ~55 days) in the SLA and OMZ-top cross-spectrum agrees with the time scales of equatorially-forced CTWs (Spillane et al., 1987; Gutiérrez et al., 2014) and suggests that the deepening during El Niño is associated with the passage of CTWs. However, north of Cabo Corrientes, inside the GCE (23 °N), the peak in the cross-spectrum disappeared, even though the propagation of CTW continued (Fig. 9). As the OMZ-top was deeper in this area (GCE), it may have been less sensitive to the dominant CTW low-order modes. Furthermore, the CGE is a transition area where other processes, such as mesoscale eddies and the presence of water masses with different properties, may influence the variability of OMZ-top.

The substantial variability of the OMZ boundary modelled in the GCE during El Niño 2015-16 appears to be related to an intensification of mesoscale dynamics (Figs. S8B, D). During OND 2015, there was an intensification in the poleward flow next to the coast, which was broad and covered the eastern half of the GC mouth. Since the intensification was not reproduced in the LFBRY simulation, it is expected that it was enhanced by the arrival of downwelling CTWs (Zamudio et al., 2008; Gómez-Valdivia et al., 2015). However, owing to the deepening of the isotherms associated with El Niño, the enhanced poleward advection of

warm, oxygenated TSW rather than oxygen-depleted StSsW took place (Fig. 12C) (Castro et al., 2000). Later, in winter 2016, the anticyclonic circulation in the GC mouth was much stronger than average (Fig 12*,* Fig. S8), causing the expulsion of the OMZ-core far more southern than the GC mouth. The OMZ boundary in the El Niño 2015-16 winter was comparable to an average summer (Fig. 8). This intensification was not reproduced in the sensitivity experiment (LFBRY), suggesting that the CTWs associated with El Niño enhanced the poleward flow related to the intensity of the anticyclonic circulation in the GCE (Gómez-Valdivia et al., 2015; Farach-Espinoza et al., 2021). El Niño events are also associated with weakening upwelling favorable winds (Herrera-Cervantes et al., 2007; Farach-Espinoza et al.,2021). However, the wind stress estimated by the model showed an increase of up to 40% of wind stress in the upper mid-GC during the 2015 fall (OND), while in JFM there was a slight decrease (< 10%) of the wind stress in the lower middle GC (not shown). Therefore, it is not expected that the OMZ-top differences could be related to differences in the upwelling rate.

Besides the discussed influence of dynamic processes on the OMZ boundary variability in the GCE, other processes, particularly biogeochemical, could also be relevant. Regarding interannual variability, El Niño events typically decrease primary productivity, while La Niña events increase it (Kahru et al., 2004; Lluch-Cota et al., 2010). These changes in primary production are expected to contribute to OMZ-top deepening or shoaling of the OMZ-top. The discussion of the biogeochemical processes involved is beyond the scope of this work and is deferred to future work.

6. Conclusions

This study highlights the dynamic behavior of the oxygen minimum zone boundary (OMZ) at the Gulf of California entrance (GCE), revealing distinct patterns of shoaling and deepening influenced by various oceanographic processes. The seasonal variability exhibits a semiannual cycle of alternate periods of shoaling and deepening of the OMZ boundary, significantly influenced by seasonal shifts of a poleward undercurrent along the coast and the following formation of an anticyclonic eddy within the GC mouth. The poleward undercurrent, which is part of the Mexican Coastal Current, shoals the OMZ upper limit and pushes the OMZ core to the GC during fall and spring. The anticyclonic eddy, occurring in winter (weaker) and summer, deepens the OMZ upper limit and forces the OMZ core out of the gulf by the continental side. The interaction between local mesoscale dynamics and remote forcings, particularly coastal-trapped waves (CTWs), plays a significant role in shaping the OMZ boundary's behavior. The study confirms that while CTWs enhance the poleward flow and intensify the anticyclonic circulation, their absence does not prevent the formation of anticyclonic eddies at the Gulf's entrance.

Interannual variability, particularly during strong El Niño and La Niña events, shows the OMZ boundary's sensitivity to changes in oceanic and atmospheric conditions. El Niño events lead to a pronounced deepening of the OMZ, driven by enhanced mesoscale activity. In contrast, La Niña events cause a shoaling effect, intensifying the OMZ's presence along the coast.

This research demonstrates the value of integrating high-resolution ocean models with observational data to unravel the complex interplay between physical and biogeochemical processes driving the OMZ variability, especially in regions with limited observational data availability. Future work should further explore the role of biogeochemical processes in OMZ dynamics, particularly under changing climatic conditions.

Funding sources

The numerical simulations were performed on the IDRIS Jean-Zay high performance computers under DARI projects A0130101140 and A0110101140. This work was also funded

by Universidad Nacional Autónoma de México (UNAM, projects PAPIIT IB201612, IN110518, IN103721and IN110624), CONAHCYT (PDCPN 214349 and SEMARNAT 278634), the International Atomic Energy Agency (Technical cooperation projects RLA7020, RLA7022, RLA7025 and RLA7028). The collaboration between UNAM and IRD is through the IRN DEXICOTROP project. Support by i) the Posgrado en Ciencias del Mar y Limnología, UNAM, ii) Sorbonne Université, École doctorale 129, Sciences de l'Environnement d'Ile de France, iii) Campus France, and a PhD fellowship from CONAHCYT (CVU No. 823599) is acknowledged by CAHB.

Acknowledgments

Cruise data from June 2015 was supported by the project lead by Laura Sánchez-Velasco (2014-236864) "Influencia de remolinos de mesoescala sobre hábitats de larvas de peces (con énfasis en especies de importancia comercial) en la zona de mínimo de oxígeno del océano Pacífico frente a México: Océano abierto y efecto de islas," the project SEP – CONACyT (#2011-168034-T) "Un estudio de la Corriente Costera Mexicana y el Pacífico adyacente, con un 'SeaGlider,' cruceros oceanográficos y datos de satélite," and the project CONACyT Fronteras de la Ciencia 180 "Probando paradigmas sobre la expansión de la zona de mínimo de oxígeno: reducción del hábitat vertical del zooplancton y su efecto en el ecosistema pelágico mediante métodos autónomos".

The long-term project Coastal Observatories of Global Change would not be possible without the institutional support received by the Direction and Administration of the Instituto de Ciencias del Mar y Limnología, UNAM through the years at the Mazatlán observatory. The authors thank the technical support provided by Benjamín Yáñez Chávez, Beatriz Yáñez Rivera and Sergio Rendón Rodríguez† (sampling), Marcela Guillermina Fregoso López, and Libia Hascibe Pérez Bernal (laboratory analysis), Carlos Suárez Gutiérrez and León Felipe Álvarez Sánchez (data management).

Credit authorship contribution statement

Carlos Alberto Herrera-Becerril: Conceptualization, Formal analysis, Software, Writing – original draft, Writing – review and editing. François Colas: Conceptualization, Formal analysis, Funding acquisition, Resources, Software, Supervision, Writing – original draft, Writing – review and editing. Joan-Albert Sanchez-Cabeza: Conceptualization, Formal analysis. Funding acquisition, Resources, Supervision, Writing – original draft, Writing – review and editing. José Martín Hernandez-Ayon: Supervision, Writing – review and editing. Vincent Echevin: Supervision, Writing – review and editing. José Gilberto Cardoso-Mohedano: Software, Supervision, Writing – review and editing. Ana Carolina Ruiz-Fernández: Funding acquisition, Resources, Writing – review and editing.

Data Statement

The CROCO-PISCES model is open-source and freely available at https://www.croco-ocean.org/. Model outputs are very large and will be made available on request to the corresponding author.

Declaration of Competing Interest

The authors declare that they have no known competing financial interests or personal relationships that could have appeared to influence the work reported in this paper.

References

Auger, P. A., Bento, J. P., Hormazabal, S., Morales, C. E., & Bustamante, A. (2021). Mesoscale variability in the boundaries of the oxygen minimum zone in the eastern

south Pacific: Influence of intrathermocline eddies. Journal of Geophysical Research: Oceans, 126(2), e2019JC015272. https://doi.org/10.1029/2019JC015272

Aumont, O., & Bopp, L. (2006). Globalizing results from ocean in situ iron fertilization studies. *Global Biogeochemical Cycles, 20*(2). https://doi.org/10.1029/2005GB002591

Aumont, O., Éthé, C., Tagliabue, A., Bopp, L., & Gehlen, M. (2015). PISCES-v2: an ocean biogeochemical model for carbon and ecosystem studies. Geoscientific Model Development, 8(2), 2465-2513. https://doi.org/10.5194/gmd-8-2465-2015

Bange, H. W. (2008). Gaseous nitrogen compounds (NO, N_2O, N_2, NH_3) in the ocean. In Capone, D. G., Bronk, D. A., Mulholland, M. R., & Carpenter, E. J. (Eds.), *Nitrogen in the Marine Environment* (2nd ed., pp. 51–94). Elsevier. B978-0-12-372522-6.00021-9

Boening, C., Willis, J. K., Landerer, F. W., Nerem, R. S., & Fasullo, J. (2012). The 2011 La Niña: So strong, the oceans fell. Geophysical Research Letters, 39(19). https://doi.org/10.1029/2012GL053055

Brandt, P., Bange, H. W., Banyte, D., Dengler, M., Didwischus, S.-H., Fischer, T., Greatbatch, R. J., Hahn, J., Kanzow, T., Karstensen, J., Körtzinger, A., Krahmann, G., Schmidtko, S., Stramma, L., Tanhua, T., & Visbeck, M. (2015). On the role of circulation and mixing in the ventilation of oxygen minimum zones with a focus on the eastern tropical North Atlantic. *Biogeosciences, 12*(2), 489–512. https://doi.org/10.5194/bg-12-489-2015

Bretagnon, M., Paulmier, A., Garçon, V., Dewitte, B., Illig, S., Leblond, N., Coppola, L., Campos, F., Velazco, F., Panagiotopoulos, C., Oschlies, A., Hernandez-Ayon, J. M., Maske, H., Vergara, O., Montes, I., Martinez, P., Carrasco, E., Grelet, J., Desprez-De-Gesincourt, O., Maes, C., & Scouarnec, L. (2018). Modulation of the vertical particle transfer efficiency in the oxygen minimum zone off Peru. Biogeosciences, 15(16), 5093-5111. https://doi.org/10.5194/bg-15-5093-2018

Castro, R., Mascarenhas, A. S., Durazo, R., & Collins, C. A. (2000). Variación estacional de la temperatura y salinidad en la entrada del Golfo de California, México. Ciencias Marinas, 26(4), 561-583. https://doi.org/10.7773/cm.v26i4.621

Cepeda-Morales, J., Gaxiola-Castro, G., Beier, E., & Godínez, V. M. (2013). The mechanisms involved in defining the northern boundary of the shallow oxygen minimum zone in the eastern tropical Pacific Ocean off Mexico. Deep Sea Research Part I: Oceanographic Research Papers, 76, 1-12. https://doi.org/10.1016/j.dsr.2013.02.004

Chelton, D. B., Schlax, M. G., & Samelson, R. M. (2011). Global observations of nonlinear mesoscale eddies. Progress in Oceanography, 91(2), 167-216. https://doi.org/10.1016/j.pocean.2011.01.002

Claustre, H., Johnson, K. S., & Takeshita, Y. (2020). Observing the global ocean with biogeochemical-Argo. Annual Review of Marine Science, 12, 23-48. https://doi.org/10.1146/annurev-marine-010419-010956

Delgadillo-Hinojosa, F., Segovia-Zavala, J. A., Huerta-Díaz, M. A., & Atilano-Silva, H. (2006). Influence of geochemical and physical processes on the vertical distribution of manganese in Gulf of California waters. Deep Sea Research Part I: Oceanographic Research Papers, 53(8), 1301-1319. https://doi.org/10.1016/j.dsr.2006.05.008

Devol, A. H., Uhlenhopp, A. G., Naqvi, S. W. A., Brandes, J. A., Jayakumar, D. A., Naik, H., Gaurin, S., Codispoti, L. A., & Yoshinari, T. (2006). Denitrification rates and excess nitrogen gas concentrations in the Arabian Sea oxygen deficient zone. Deep Sea Research Part I: Oceanographic Research Papers, 53(9), 1533-1547. https://doi.org/10.1016/j.dsr.2006.07.005

Diaz, R. J., & Rosenberg, R. (2008). Spreading dead zones and consequences for marine ecosystems. Science, 321(5891), 926-929. https://doi.org/10.1126/science.1156401

Espinoza-Morriberón, D., Echevin, V., Colas, F., Tam, J., Gutiérrez, D., Graco, M., Ledesma, J., & Quispe-Ccalluari, C. (2019). Oxygen variability during ENSO in the tropical South Eastern Pacific. Frontiers in Marine Science, 5, 526. https://doi.org/10.3389/fmars.2018.00526

Farach-Espinoza, E. B., López-Martínez, J., García-Morales, R., Nevárez-Martínez, M. O., Lluch-Cota, D. B., & Ortega-García, S. (2021). Temporal variability of oceanic mesoscale events in the Gulf of California. Remote Sensing, 13(9), 1774. https://doi.org/10.3390/rs13091774

Flores-Morales, A. L., Parés-Sierra, A., & Gómez-Valdivia, F. (2012). Semiannual Kelvin waves in the northeastern tropical Pacific. Journal of Coastal Research, 28(5), 1068-1072. https://doi.org/10.2112/JCOASTRES-D-11-00196.1

Flores-Vidal, X., Durazo, R., Zavala-Sansón, L., Flament, P., Chavanne, C., Ocampo-Torres, F. J., & Reyes-Hernández, C. (2014). Evidence of inertially generated coastal-trapped waves in the eastern tropical Pacific. Journal of Geophysical Research: Oceans, 119(5), 3121-3133. https://doi.org/10.1002/2013JC009118

Fuenzalida, R., Schneider, W., Garcés-Vargas, J., Bravo, L., & Lange, C. (2009). Vertical and horizontal extension of the oxygen minimum zone in the eastern South Pacific Ocean. Deep Sea Research Part II: Topical Studies in Oceanography, 56(16), 992-1003. https://doi.org/10.1016/j.dsr2.2008.11.001

Gallo, N. D., & Levin, L. A. (2016). Fish ecology and evolution in the world's oxygen minimum zones and implications of ocean deoxygenation. Advances in marine biology, 74, 117-198. https://doi.org/10.1016/bs.amb.2016.04.001

Garcia, H.E., Z. Wang, C. Bouchard, S.L. Cross, C.R. Paver, J.R. Reagan, T.P. Boyer, R.A. Locarnini, A.V. Mishonov, O. Baranova, D. Seidov, and D. Dukhovskoy (2024). World Ocean Atlas 2023, Volume 3: Dissolved Oxygen, Apparent Oxygen Utilization, and Oxygen Saturation. A. Mishonov, Tech. Ed. NOAA Atlas NESDIS 91. https://doi.org/10.25923/rb67-ns53

Global Ocean Physics Reanalysis E.U. Copernicus Marine Service Information (CMEMS). Marine Data Store (MDS). DOI: https://doi.org/10.48670/moi-00021 (Accessed on 08 Feb 2023)

Godínez, V. M., Beier, E., Lavín, M. F., & Kurczyn, J. A. (2010). Circulation at the entrance of the Gulf of California from satellite altimeter and hydrographic observations. Journal of Geophysical Research: Oceans, 115(C4). https://doi.org/10.1029/2009JC005705

Gómez-Valdivia, F., Parés-Sierra, A., & Flores-Morales, A. L. (2015). The Mexican Coastal Current: A subsurface seasonal bridge that connects the tropical and subtropical Northeastern Pacific. Continental Shelf Research, 110, 100-107. https://doi.org/10.1016/j.csr.2015.10.010

Good, S., Fiedler, E., Mao, C., Martin, M.J., Maycock, A., Reid, R., Roberts-Jones, J., Searle, T., Waters, J., While, J., & Worsfold, M. (2020) The Current Configuration of the OSTIA System for Operational Production of Foundation Sea Surface Temperature and Ice Concentration Analyses. Remote Sens. 12, 720. https://doi.org/10.3390/rs12040720

Gutiérrez, M. O., López, M., Candela, J., Castro, R., Mascarenhas, A., & Collins, C. A. (2014). Effect of coastal-trapped waves and wind on currents and transport in the Gulf of California. Journal of Geophysical Research: Oceans, 119(8), 5123-5139. https://doi.org/10.1002/2013JC009538

Helly, J. J., & Levin, L. A. (2004). Global distribution of naturally occurring marine hypoxia on continental margins. Deep Sea Research Part I: Oceanographic Research Papers, 51(9), 1159-1168. https://doi.org/10.1016/j.dsr.2004.03.009

Herrera-Becerril, C. A., Sanchez-Cabeza, J. A., Sánchez, L. F. Á., Lara-Cera, A. R., Ruiz-Fernández, A. C., Cardoso-Mohedano, J. G., ... & Colas, F. (2022). Statistical

identification of coastal hypoxia events controlled by wind-induced upwelling. Continental Shelf Research, 233, 104634. https://doi.org/10.1016/j.csr.2021.104634
Herrera-Cervantes, H., Lluch-Cota, D. B., Lluch-Cota, S. E., & Gutiérrez-de-Velasco S, G. (2007). The ENSO signature in sea-surface temperature in the Gulf of California. Journal of Marine Research, 65(5), 589-605. https://doi.org/10.1357/002224007783649529
Hersbach, H., Bell, B., Berrisford, P., Biavati, G., Horányi, A., Muñoz Sabater, J., Nicolas, J., Peubey, C., Radu, R., Rozum, I., Schepers, D., Simmons, A., Soci, C., Dee, D., Thépaut, J-N. (2018): ERA5 hourly data on single levels from 1979 to present. Copernicus Climate Change Service (C3S) Climate Data Store (CDS). https://doi.org/10.24381/cds.adbb2d47
Hilt, M., Roblou, L., Nguyen, C., Marchesiello, P., Lemari e, F., Jullien, S., Dumas, F., Debreu, L., Capet, X., Bordois, L., Benshila, R., Auclair, F., 2020. Numerical modeling of hydraulic control, solitary waves and primary instabilities in the Strait of Gibraltar. Ocean Model. 151 (16p), 101642. https://doi.org/10.1016/j.ocemod.2020.101642
Hofmann, A. F., Peltzer, E. T., Walz, P. M., & Brewer, P. G. (2011). Hypoxia by degrees: Establishing definitions for a changing ocean. Deep Sea Research Part I: Oceanographic Research Papers, 58(12), 1212-1226. https://doi.org/10.1016/j.dsr.2011.09.004
Kahru, M., Marinone, S. G., Lluch-Cota, S. E., Parés-Sierra, A., & Mitchell, B. G. (2004). Ocean-color variability in the Gulf of California: scales from days to ENSO. Deep Sea Research Part II: Topical Studies in Oceanography, 51(1-3), 139-146. https://doi.org/10.1016/j.dsr2.2003.04.001
Kalvelage, T., Lavik, G., Jensen, M. M., Revsbech, N. P., Löscher, C., Schunck, H., Desai, D., Hauss, H., Kiko, R., Holtappels, M., LaRoche, J., Schmitz, R. A., Graco, M. I., & Kuypers, M. M. (2015). Aerobic microbial respiration in oceanic oxygen minimum zones. PLOS ONE, 10(7), e0133526. https://doi.org/10.1371/journal.pone.0133526
Karstensen, J., Stramma, L., & Visbeck, M. (2008). Oxygen minimum zones in the eastern tropical Atlantic and Pacific oceans. Progress in Oceanography, 77(4), 331-350. https://doi.org/10.1016/j.pocean.2007.05.009
Kessler, W. S. (2006). The circulation of the eastern tropical Pacific: A review. Progress in Oceanography, 69(2-4), 181-217. https://doi.org/10.1016/j.pocean.2006.03.009
Kurczyn, J. A., Beier, E., Lavín, M. F., & Chaigneau, A. (2012). Mesoscale eddies in the northeastern Pacific tropical-subtropical transition zone: Statistical characterization from satellite altimetry. Journal of Geophysical Research: Oceans, 117(C10). https://doi.org/10.1029/2012JC007970
Large, W. G., McWilliams, J. C., & Doney, S. C. (1994). Oceanic vertical mixing: A review and a model with a nonlocal boundary layer parameterization. Reviews of Geophysics, 32(4), 363-403. https://doi.org/10.1029/94RG01872
Lavín, M. F., & Marinone, S. G. (2003). An overview of the physical oceanography of the Gulf of California. Nonlinear Processes in Geophysical Fluid Dynamics: A tribute to the scientific work of Pedro Ripa, 173-204. https://doi.org/10.1007/978-94-010-0074-1_11
Lavín, M. F., Castro, R., Beier, E., Godínez, V. M., Amador, A., & Guest, P. (2009). SST, thermohaline structure, and circulation in the southern Gulf of California in June 2004 during the North American Monsoon Experiment. Journal of Geophysical Research: Oceans, 114(C2). https://doi.org/10.1029/2008JC004896
Lavín, M. F., Castro, R., Beier, E., & Godínez, V. M. (2013). Mesoscale eddies in the southern Gulf of California during summer: Characteristics and interaction with the

wind stress. Journal of Geophysical Research: Oceans, 118(3), 1367-1381. https://doi.org/10.1002/jgrc.20132

Lemarié, F., Kurian, J., Shchepetkin, A. F., Molemaker, M. J., Colas, F., & McWilliams, J. C. (2012). Are there inescapable issues prohibiting the use of terrain-following coordinates in climate models? Ocean Modelling, 42, 57-79. https://doi.org/10.1016/j.ocemod.2011.11.007

Liang, J. H., McWilliams, J. C., Kurian, J., Colas, F., Wang, P., & Uchiyama, Y. (2012). Mesoscale variability in the northeastern tropical Pacific: Forcing mechanisms and eddy properties. Journal of Geophysical Research: Oceans, 117(C7). https://doi.org/10.1029/2012JC008008

Lluch-Cota, S. E., Parés-Sierra, A., Magaña-Rueda, V. O., Arreguín-Sánchez, F., Bazzino, G., Herrera-Cervantes, H., & Lluch-Belda, D. (2010). Changing climate in the Gulf of California. Progress in Oceanography, 87(1-4), 114-126. https://doi.org/10.1016/j.pocean.2010.09.007

Márquez-Artavia, A., Sánchez-Velasco, L., Barton, E. D., Paulmier, A., Santamaría-Del-Ángel, E., & Beier, E. (2019). A suboxic chlorophyll-a maximum persists within the Pacific oxygen minimum zone off Mexico. Deep Sea Research Part II: Topical Studies in Oceanography, 169, 104686. https://doi.org/10.1016/j.dsr2.2019.104686

McCoy, D., Damien, P., Clements, D., Yang, S., & Bianchi, D. (2023). Pathways of nitrous oxide production in the eastern tropical south pacific oxygen minimum zone. Global Biogeochemical Cycles, 37(7), e2022GB007670. https://doi.org/10.1029/2022GB007670

Páez-Osuna, F., Sanchez-Cabeza, J. A., Ruiz-Fernández, A. C., Alonso-Rodríguez, R., Piñón-Gimate, A., Cardoso-Mohedano, J. Flores-Verdugo, F., Carballo, J. L., Cisneros-Mata, M. Á., & Álvarez-Borrego, S. (2016). Environmental status of the Gulf of California: A review of responses to climate change and climate variability. Earth-Science Reviews, 162, 253–268. https://doi.org/10.1016/j.earscirev.2016.09.015

Pantoja, D. A., Marinone, S. G., Parés-Sierra, A., & Gómez-Valdivia, F. (2012). Modelación numérica de la hidrografía y circulación estacional y de mesoescala en el Pacífico central mexicano. Ciencias marinas, 38(2), 363-379. https://doi.org/10.7773/cm.v38i2.2007

Paulmier, A., & Ruiz-Pino, D. (2009). Oxygen minimum zones (OMZs) in the modern ocean. Progress in Oceanography, 80(3-4), 113-128. https://doi.org/10.1016/j.pocean.2008.08.001

Pegau, W. S., Boss, E., & Martínez, A. (2002). Ocean color observations of eddies during the summer in the Gulf of California. Geophysical Research Letters, 29(9), 6-1. https://doi.org/10.1029/2001GL014076

Penven, P., Cambon, G., Marchesiello, P., Sepulveda, A., Benshila, R., Illig, S., Jullien, S., Le Gentil, S., Le Corre, M., Morvan, G., & Rougier, G. (2019). CROCO tools (1.1). Zenodo. https://doi.org/10.5281/zenodo.7432028

Penven, P., Debreu, L., Marchesiello, P., & McWilliams, J. C. (2006). Evaluation and application of the ROMS 1-way embedding procedure to the central California upwelling system. Ocean Modelling, 12(1-2), 157-187. https://doi.org/10.1016/j.ocemod.2005.05.002

Portela, E., Beier, E., Barton, E. D., Castro, R., Godínez, V., Palacios-Hernández, E., ... & Trasviña, A. (2016). Water masses and circulation in the tropical Pacific off central Mexico and surrounding areas. Journal of Physical Oceanography, 46(10), 3069-3081. https://doi.org/10.1175/jpo-d-16-0068.1

Pujol, M. I., Faugère, Y., Taburet, G., Dupuy, S., Pelloquin, C., Ablain, M., & Picot, N. (2016). DUACS DT2014: the new multi-mission altimeter data set reprocessed over 20 years. Ocean Science, 12(5), 1067-1090. https://doi.org/10.5194/os-12-1067-2016

Reagan, James R.; Boyer, Tim P.; García, Hernán E.; Locarnini, Ricardo A.; Baranova, Olga K.; Bouchard, Courtney; Cross, Scott L.; Mishonov, Alexey V.; Paver, Christopher R.; Seidov, Dan; Wang, Zhankun; Dukhovskoy, Dmitry. (2024). World Ocean Atlas 2023. NOAA National Centers for Environmental Information. https://doi.org/10.25923/rb67-ns53

Resplandy, L., Lévy, M., Bopp, L., Echevin, V., Pous, S. V. V. S. S., Sarma, V. V. S. S., & Kumar, D. (2012). Controlling factors of the oxygen balance in the Arabian Sea's OMZ. Biogeosciences, 9(12), 5095-5109. https://doi.org/10.5194/bg-9-5095-2012

Sanchez-Cabeza, J. A., Herrera-Becerril, C. A., Carballo, J. L., Yáñez, B., Álvarez-Sánchez, L. F., Cardoso-Mohedano, J. G., & Ruiz-Fernández, A. C. (2022). Rapid surface water warming and impact of the recent (2013–2016) temperature anomaly in shallow coastal waters at the eastern entrance of the Gulf of California. Progress in Oceanography, 202, 102746. https://doi.org/10.1016/j.pocean.2022.102746

Sánchez-Pérez, E. D., Sánchez-Velasco, L., Ruvalcaba-Aroche, E. D., Ornelas-Vargas, A., Beier, E., Barton, E. D., ... & Contreras-Catala, F. (2021). Temperature and dissolved oxygen concentration in the Pacific Ocean at the northern region of the oxygen minimum zone off Mexico between the last two PDO cool phases. Journal of Marine Systems, 222, 103607. https://doi.org/10.1016/j.jmarsys.2021.103607

Sánchez-Velasco, L., Beier, E., Godínez, V. M., Barton, E. D., Santamaría-del-Angel, E., Jiménez-Rosemberg, S. P. A., & Marinone, S. G. (2017). Hydrographic and fish larvae distribution during the "Godzilla El Niño 2015–2016" in the northern end of the shallow oxygen minimum zone of the Eastern Tropical Pacific Ocean. Journal of Geophysical Research: Oceans, 122(3), 2156-2170. https://doi.org/10.1002/2016JC012622

Shchepetkin, A. F., & McWilliams, J. C. (2005). The regional oceanic modeling system (ROMS): a split-explicit, free-surface, topography-following-coordinate oceanic model. Ocean Modeling, 9(4), 347-404. https://doi.org/10.1016/j.ocemod.2004.08.002

Shchepetkin, A. F., & McWilliams, J. C. (2009). Computational kernel algorithms for fine-scale, multiprocess, longtime oceanic simulations. In Handbook of Numerical Analysis (Vol. 14, pp. 121-183). Elsevier. https://doi.org/10.1016/S1570-8659(08)01202-0

Smith, W. H., & Sandwell, D. T. (1997). Global sea floor topography from satellite altimetry and ship depth soundings. Science, 277(5334), 1956-1962. 10.1126/science.277.5334.1956

Spillane, M. C., Enfield, D. B., & Allen, J. S. (1987). Intraseasonal oscillations in sea level along the west coast of the Americas. Journal of Physical Oceanography, 17(3), 313-325. https://doi.org/10.1175/1520-0485(1987)017<0313:IOISLA>2.0.CO;2

Stramma, L., Johnson, G. C., Sprintall, J., & Mohrholz, V. (2008). Expanding oxygen-minimum zones in the tropical oceans. science, 320(5876), 655-658. 10.1126/science.1153847

Tegen, I., & Fung, I. (1995). Contribution to the atmospheric mineral aerosol load from land surface modification. Journal of Geophysical Research: Atmospheres, 100(D9), 18707-18726. https://doi.org/10.1029/95JD02051

Trucco-Pignata, P. N., Hernández-Ayón, J. M., Santamaria-del-Angel, E., Beier, E., Sánchez-Velasco, L., Godínez, V. M., & Norzagaray, O. (2019). Ventilation of the upper oxygen minimum zone in the coastal region off Mexico: implications of El Niño 2015–2016. Frontiers in Marine Science, 6, 459. https://doi.org/10.3389/fmars.2019.00459

Vergara, O., Dewitte, B., Montes, I., Garçon, V., Ramos, M., Paulmier, A., & Pizarro, O. (2016). Seasonal variability of the oxygen minimum zone off Peru in a high-resolution regional coupled model. Biogeosciences, 13(15), 4389-4410. https://doi.org/10.5194/bg-13-4389-2016

Ward, B. B., Devol, A. H., Rich, J. J., Chang, B. X., Bulow, S. E., Naik, H., Pratihary, A., & Jayakumar, A. (2009). Denitrification as the dominant nitrogen loss process in the Arabian Sea. Nature, 461(7260), 78-81. https://doi.org/10.1038/nature08276

Willmott, C. J. (1981). On the Validation of Models. Physical Geography, 2(2), 184–194. https://doi.org/10.1080/02723646.1981.10642213

Zamudio, L., Hogan, P., & Metzger, E. J. (2008). Summer generation of the Southern Gulf of California eddy train. Journal of Geophysical Research: Oceans, 113(C6). https://doi.org/10.1029/2007JC004467